Biomechanical tensile behavior of human Wharton's jelly

Adrien Baldit, Marie Dubus, Johan Sergheraert, Halima Kerdjoudj, Cedric
Mauprivez, Rachid Rahouadj

▶ **To cite this version:**

HAL Id: hal-03480413
https://hal.univ-reims.fr/hal-03480413

Submitted on 8 Jan 2024

Research Paper

Biomechanical tensile behavior of human Wharton's jelly

Adrien Baldit[a,b,*], Marie Dubus[c], Johan Sergheraert[c,d], Halima Kerdjoudj[c], Cedric Mauprivez[c,d], Rachid Rahouadj[a]

[a]*LEM3-UMR-7239, CNRS - Université de Lorraine - Arts et Métiers ParisTech, FRANCE*
[b]*ENIM, Université de Lorraine, METZ, FRANCE*
[c]*Université de Reims Champagne Ardenne, Biomatériaux et Inflammation en Site Osseux (BIOS) EA 4691, 51100, Reims, France*
[d]*Centre Hospitalier Universitaire de Reims, France*

Abstract

Wharton's jelly (WJ) is a mucous connective tissue of the umbilical cord. It shows high healing capabilities, mainly attributed to the chemical composition and to the presence of stem cells, growth factors and peptides. Although WJ biological properties are well documented in vitro and in vivo, there is still a lack of mechanical data on this tissue, which is paramount for its use as a biomaterial for medical applications. In this study, mechanical responses of ten WJ samples within close physiological conditions were registered undergoing quasi static cyclic tensile tests followed by a load up to failure. This protocol aimed on one hand to provide biomechanical data to feed predictive numerical models and on the other hand increase WJ knowledge in view of its potential use in biomedical field. In spite of the WJ harvest, the resulting viscous nonlinear elastic response obtained is fully in tune with the literature confirming the database quality. A side of the knowledge improvement on WJ mechanical response, this paper provides accurate data that will enhance predictive simulation work such as finite element analysis. The mechanical step-through brought by the analytical nonlinear characterization over cyclic and ultimate loads is to predict WJ behavior. Actually, principal component analysis highlighted its quality while pointing out indicators, such as failure or hydration criteria, as well as models' limitations.
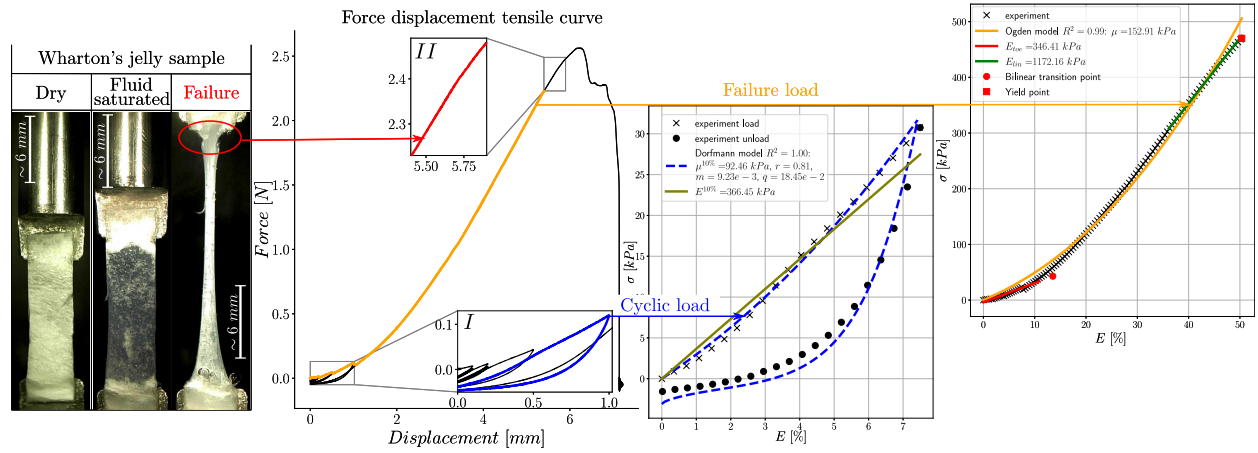
Keywords:
Warthon's jelly, Biomechanics, Hyperelasticity, Viscosity, Cyclic tensile characterization, Failure

---

*Corresponding author
Email address:* `adrien.baldit@univ-lorraine.fr` (Adrien Baldit)

Graphical abstract

Highlights

- Predictive biomechanical models for biomaterials dedicated to medical applications.

- Cyclic and ultimate tensile responses of ten Wharton's jelly samples within close physiological conditions.

- Wharton's jelly cyclic response fitted thanks to nonlinear hyperelastic models.

- Wharton's jelly mechanical repetitiveness confirms the interest for regenerative medicine.

- Principal component analysis highlighted predictive indicators.

1. Introduction

Over the last decades, a great importance has been given to the use of biological derived tissue for regenerative medicine applications (Fernandez, 2019; Koči et al., 2017; Safari et al., 2019). Among these tissues, perinatal tissues such as umbilical cord are easily accessible and available as opposed to other biologics. While earlier numerous clinical studies showed that umbilical cord blood has great therapeutical effect in hematopoietic disorders and in cancer treatment (Gluckman et al., 1989; Knudtzon, 1974), the solid tissues of umbilical cord have been considered for a while as a valueless medical waste. The past decade, however, has been notable for intensive development of biomedical products and biologics on the basis of umbilical cord tissues such as Wharton's jelly (WJ) derived mesenchymal stem cells (i.e. intended for the treatment of cardiovascular, liver, and skeletal muscle failures, autoimmune and neurological disorders, and many other diseases), umbilical cord vessels (i.e. as grafts for vascular surgery) and Wharton's jelly-derived extracellular matrix (i.e. for wound healing) (Caputo et al., 2016; Marston et al., 2019; Raphael, 2016; Tettelbach et al., 2019). WJ is a mucous connective tissue, located between the amniotic membrane and the umbilical vessels, showing high healing capabilities, mainly attributed to the chemical composition (i.e. collagen and

glycosaminoglycanes) and to the presence of stem cells, growth factors and peptides (Gupta et al., 2020; Herndon and Branski, 2017; John et al., 2019; Mechiche Alami et al., 2014). Furthermore, WJ, described as a three-dimensional spongy network of collagenous fibers and glycoprotein microfibrils with a random arrangement (Pennati, 2001), provides a structural and mechanical support to umbilical vessels by preventing their compression, torsion, and bending (Gervaso et al., 2014; Mallis et al., 2020). Although WJ biological properties are well documented in vitro and in vivo, there is still a lack of mechanical data on this tissue, which is paramount for its use as a biomaterial for medical applications aimed by this work. Nonetheless the already published studies contain important information regarding mechanical loading protocols and first parameters' values within the linear elastic framework.

The work of Pennati (2001) highlighted WJ nonlinear stress strain response undergoing tensile load. In the same paper, the author stated a yield point at 22% strain correlated to 1.29 MPa stress. A bilinear characterization led to "toe" and "linear" elastic moduli respectively equal to $E_{toe} = 0.9\ MPa$ and $E_{lin} = 11.1\ MPa$ for both linear regions' behaviors. This strengthening has been associated, on the one hand, to low strain loading on the microfibril network, described by E_{toe}. On the other hand, the collagen fibers, not stretched within toe region, are recruited through large strain load showing a second linear behavior, represented by E_{lin}. The viscous behavior of the WJ has been observed through relaxation tests (Pennati, 2001) and confirmed by the poro-elastic characterization made by Gervaso et al. (2014). In this last work, they measured WJ aggregate modulus, permeability and porosity. This latter property was measured in a range of 88.3% to 93.5% suggesting its high water content. The mechanical characterization led to a Young modulus around 4.5 kPa and a Poisson ratio around 0.47. The different values of elastic moduli between these summarized works have been attributed to the role of the fibers that are not playing a major mechanical role while compressed. Also, the different initial loading conditions, between both experiment types, potentially affects the WJ response due to its nonlinear behavior. This literature review led to mainly find linear elastic parameter values while works already exist dealing with non-linear characterisation of the umbilical cord vein and arteries (Karimi and Navidbakhsh, 2014). It also points out the missing data for computational modeling (Brunelli et al., 2019).

The composition of WJ was given by deoxyribonucleic acid (DNA) quantification and histological characterization of collagen as well as glycosaminoglycanes (GAGs). Aiming a poro-visco-elastic characterization of the WJ, a protocol has been developed to measure as many phenomena as possible without changing the test sample to limit discrepancies due to donor variability and sample location as well as possible local heterogeneous properties (Baldit et al., 2014; Franceschini et al., 2006; Tappert et al., 2018). Therefore, mechanical responses of ten WJ samples within close physiological conditions were registered undergoing quasi static cyclic tensile tests followed by a load up to failure. Mechanical properties have been assessed using linear approach as well as the classical Ogden hyperelastic model (Ogden, 1972) to reproduce experimental results comparable to literature and enhanced by a nonlinear approach. This non-linear behavior law has been chosen because it is very well known and implemented in many simulation software. It allows then easy comparison and opens on various perspectives of modeling improvements. Besides, to the best of our knowledge, a first fitting of the WJ cyclic response has been obtained thanks to the Ogden's model extension introduced by Dorfmann and Ogden (2004). Eventually, the large amount of results has been

55   analyzed through Pearson's correlation coefficient matrices and Principal Component Analysis (PCA) to enrich the

56   discussion mainly regarding the chosen models' pertinence and limitations.

57   This work aimed on the one hand to provide biomechanical data to feed predictive numerical models and on the other

58   hand increase WJ knowledge in view of its potential use in biomedical field.

2. Material and methods

2.1. Samples

61   Five fresh human umbilical cords, obtained after full-term births, have been collected thanks to a procedure eth-

62   ically and methodologically approved by our local Research Institution and was conducted with informed patients

63   (written consent) in accordance with the usual ethical legal regulations (Article R 1243-57, in accordance with our

64   authorization and registration number DC-2014-2262 given by the French institutions). Medial portions of umbilical

65   cords were washed several times with distilled water to remove blood components and stored at -20^oC until pro-

66   cessing. Defrosted umbilical cord were dissected using surgical scissor and vascular structures were removed using

67   surgical forceps. Wharton's jelly matrix was then carefully peeled off the amniotic surrounding membrane, and freeze-

68   dried without dissociating core and peripheral locations due to sample extraction complexity. For each extirpated WJ

69   membrane, samples were cut with scalpel blade.

2.2. Biological assessment

71   DNA was extracted from five WJ membranes using MasterPure^{TM} DNA Purification Kit (Epicentre® Biotech-

72   nologies) in accordance with the manufacturer protocol. Samples were weighed prior to DNA extraction. Extracted

73   DNA was measured using Nanodrop® , Thermo Scientific with 260/280 *nm* absorbance ratio for all measured sam-

74   ples comprised between 1.8 and 2.0. Quantified DNA was normalized to the tissue weigh. Histological analysis of

75   WJ samples were performed on 4 *μm* sections of sample-embedded paraffin (rotation microtome RM2055, Leica Mi-

76   crosystems). Hematoxylin-Eosin-Saffron (HES) and Alcian blue staining were performed separately on consecutive

77   tissue sections and images were taken using scanner iScan Coreo AU scanner (Roche® , Ventana).

2.3. Mechanical assessment

79   In total ten WJ samples were collected for mechanical tests: two per WJ membrane. They were weighed thanks

80   to a Sartorius CPA225D scale (reproducibility ±50 *μg*) while optical measurements (digital microscope camera usb,

81   9.0 *Mp*, 200×, Oowl Tech Ltd) allowed assessing dimensions and subsequently giving the dry density ρ. The tensile

82   tests were carried out thanks to a universal tensile machine (Zwicky 0.5) equipped with a 10 *N* load cell. To perform

83   tests in close physiological conditions, a tank has been adapted to the machine with specific jaws (Tappert et al.,

84   2018). It required 6 *mm* diameter cylinder with flat spots as sample holder. About 2 *mm* WJ samples' length was

85   glued with cyanoacrylate on both ends (visible on figure 2) and excluded of the forth coming sample length. Once

immersed in physiological solution (Phosphate Buffer Solution, Gibco, France) maintained at 37^oC in the mechanical testing machine tank, the length of the samples increased. Therefore, the hydrated sample's length and width have been optically assessed a posteriori thanks to pictures recorded with a perpendicularly oriented camera with respect to the loading direction (Baldit et al., 2014). Consequently, a relative length variation Δl has been introduced in term of dry length percent. The average test samples' dimensions were $1.01 \pm 0.26 \times 4.69 \pm 0.44 \times 11.98 \pm 0.31$ mm^3 ($mean \pm SD$) for thickness, width and length L_0. The material parameters' average values are gathered within the table 1. As introduced, the mechanical loading aimed at characterizing the full tensile mechanical behavior range until failure under quasi static loading. Therefore, the protocol was divided into 5 steps:

1. The sample was fixed in the tensile machine then the tank was filled and the sample has been given 5 *min* to reach hydro-chemo-mechanical equilibrium (i.e. a stable force measured at the lowest load cell limit around 0.01 *N*). At the end of this stage, the hydrated length L_0 was measured leading to relative length variation Δl.

2. A preload of 0.05 *N* was applied to ensure the tensile state of the sample.

3. Subsequently, 1 %, 2 % and 5 % engineering strain cyclic loads were progressively imposed to control the mechanical response quality (smooth, nonlinear curve with hysteresis) before the following steps dedicated to mechanical characterization.

4. Then, one cycle with 10 % engineering strain was applied,

5. Eventually, a load until failure was performed with a maximum value defined either by sample failure or machine limit (i.e. 10 *N* even though this latter limit has not been reached).

As the length increased during sample hydration and was measured a posteriori, the imposed strains defined above were in fact over estimated. For the step 4, the imposed strain average value was 7.66 ± 0.50 % instead of 10 %. All loads were performed at 0.01 $mm.s^{-1}$ to fulfil the quasi static condition. After mechanical testing, the biggest remaining piece of each sample has been harvested and dried for 48*h* at 37^oC to measure the solid matrix mass m_d. Then, they were re-hydrated being immersed in physiological solution for 20*h*. Finally, their hydrated masses m_h were weighed giving the porosity φ: (Gervaso et al., 2014)

$$\varphi = \frac{m_h - m_d}{m_h} \tag{1}$$

The nominal stress σ, the Green Lagrange strain E and the stretch λ were computed from the measured data such as:

$$\sigma = \frac{F}{S_0} \quad , \quad E = \frac{1}{2}\left(\lambda^2 - 1\right) \quad and \quad \lambda = \frac{L}{L_0} \tag{2}$$

where F is the measured force for the sample length L while L_0 and S_0 are respectively the hydrated sample initial length and cross section. The characterization developed in this study has been focused only on the two last steps (i.e. 4: a 10 % strain loading cycle and 5: the loading up to sample failure). As a first approach, effective toe, E_{toe}, and linear, E_{lin}, elastic moduli were extracted through a bilinear characterization similarly to (Pennati, 2001). The transition point in between the two regions is defined by the stress-strain couple (σ_T; E_T). Then, the experimental

stress strain curves have been fitted thanks to the Ogden (1972) hyperelastic model with the following strain energy density potential W function of principal stretches λ_i:

$$W(\lambda_1, \lambda_2, \lambda_3) = \sum_{i=1}^{M} \mu_i \left(\lambda_1^{\alpha_i} + \lambda_2^{\alpha_i} + \lambda_3^{\alpha_i} - 3 \right) / \alpha_i \quad and \quad \mu = \frac{1}{2} \sum_{i=1}^{M} \mu_i \alpha_i \tag{3}$$

where μ_i and α_i are fitting parameters while μ is the shear modulus. In this study, M has been taken equal to 3 leading to six parameters to reproduce the hyperelastic response (μ_1, α_1, μ_2, α_2, μ_3 and α_3).

The Biot stress, in this uni directional stretch λ case, can be compared to the nominal stress σ such as: (Dorfmann and Ogden, 2004; Franceschini et al., 2006)

$$\sigma = \sum_{i=1}^{M} \mu_i \left(\lambda^{\alpha_i - 1} - \lambda^{-\alpha_i/2 - 1} \right) \tag{4}$$

To take into account the hysteresis appearing while unloading the material, the extension proposed by Dorfmann and Ogden (2004) has been used with a stress defined by:

$$\sigma = \eta_1 \sum_{i=1}^{M} \mu_i \left(\lambda^{\alpha_i - 1} - \lambda^{-\alpha_i/2 - 1} \right) + (1 - \eta_2) \left(\nu_1 \lambda - \bar{\nu}_2 \lambda^{-2} \right) \tag{5}$$

On primary loading $\eta_1 = \eta_2 = 1$ while on unloading and subsequent phases they are:

$$\eta_1 = 1 - \frac{1}{r} \tanh \left[\frac{W_m - W_0(\lambda)}{\mu.m} \right] \quad and \quad \eta_2 = \tanh \left[\left(\frac{W_0(\lambda)}{W_m} \right) \alpha(W_m) \right] / \tanh(1) \tag{6}$$

where $W_0(\lambda)$ and W_m are respectively the strain energy density on primary loading and its maximum value. r and m are fitting parameters while the exponent α has been kept as proposed: $\alpha = 0.3 + 0.16 W_m / \mu$ by Dorfmann and Ogden (2004). Besides, ν_1 and $\bar{\nu}_2$ are defined as:

$$\nu_1 = q.\mu \left[1 - \frac{1}{3.5} \tanh \left(\frac{\lambda_m - 1}{0.1} \right) \right] \quad and \quad \bar{\nu}_2 = q.\mu \tag{7}$$

where q is a fitting parameter and λ_m is the maximal tensile stretch imposed. Adding three parameters (r, m and q), in total nine ($M \times 2 + 3 = 9$) were required to describe a full 10 % strain load cycle taking into account the hysteresis (i.e. viscous behavior). Therefore, data were post-processed thanks to a Python script to obtain: the stress strain curves, the elastic moduli for toe and linear regions, the hyperelastic fitting (Appendix A gives the procedure quality compared to Dorfmann and Ogden (2004) work) as well as the statistical analysis. Constrained optimization by linear approximation (COBYLA from Scipy) has been used to ensure consistent parameters' values. The database here after presented is available on `zenodo.org` (currently under embargo and available as soon as the work is accepted).

3. Results

Nucleic moieties from WJ were equal to 18.40 ± 5.39 $ng/mg/\mu L$ (mean $\pm$ SD, $n = 5$). HES and Alcian blue stainings indicated a porous structure rich in collagen (red color) and glycosaminoglycan (blue color) as presented in the following figure 1.
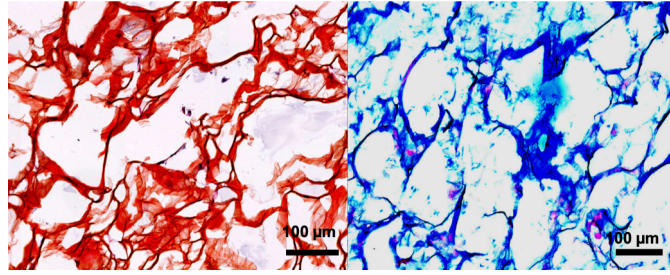
Figure 1: HES stainings (left) and alcian blue (right) stainings of two consecutive 4 *μm* WJ sections

The porosity values φ was recorded to $83.93 \pm 2.46\%$ thanks to equation 1. Preparing the mechanical test, progressive transparency while hydration has been observed for all samples and shown on figures 2.a and 2.b. Comparing these states, the relative variation of length, Δl, recorded in table 1 can be appreciated.
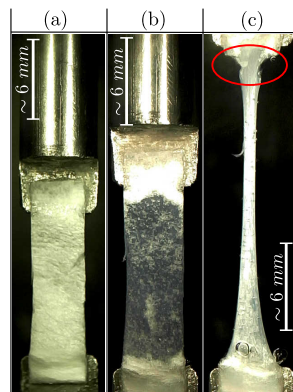

Figure 2: Sample visual aspects for a) dry, b) hydrated and c) hydrated failure states. The red encircled zone highlights the sample failure location.

During mechanical loading, the camera allowed caching the sample failure profile as presented on figure 2.c mostly occurring at an end. A representative sample's mechanical response is illustrated by the force displacement curve on figure 3.
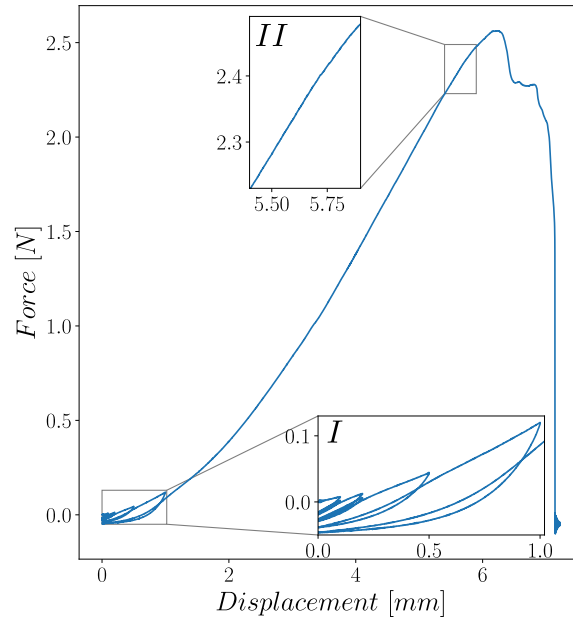
Figure 3: Representative force displacement curve (sample 160206_E4). The inset *I* points out the elastic and viscous behavior of the WJ sample through cyclic loading. On the other hand, the inset *II* shows the sample's yielding point with a concavity change.

Herein, WJ samples have a nonlinear behavior, highlighting through cycles elastic and viscous characteristics (figure 3). The former statement is based on a constant and almost continuous loading phase from step 1 to 5. The latter is comforted by the loading cycles with hysteresis that can be appreciated on the figure 3 inset *I*. The second inset points out what has been considered as the sample failure. This yielding point is obtained when the curve either changes concavity or presents a disruption. It is considered to be related to the ignition of the damage process of which the last step is shown in figure 2.c.
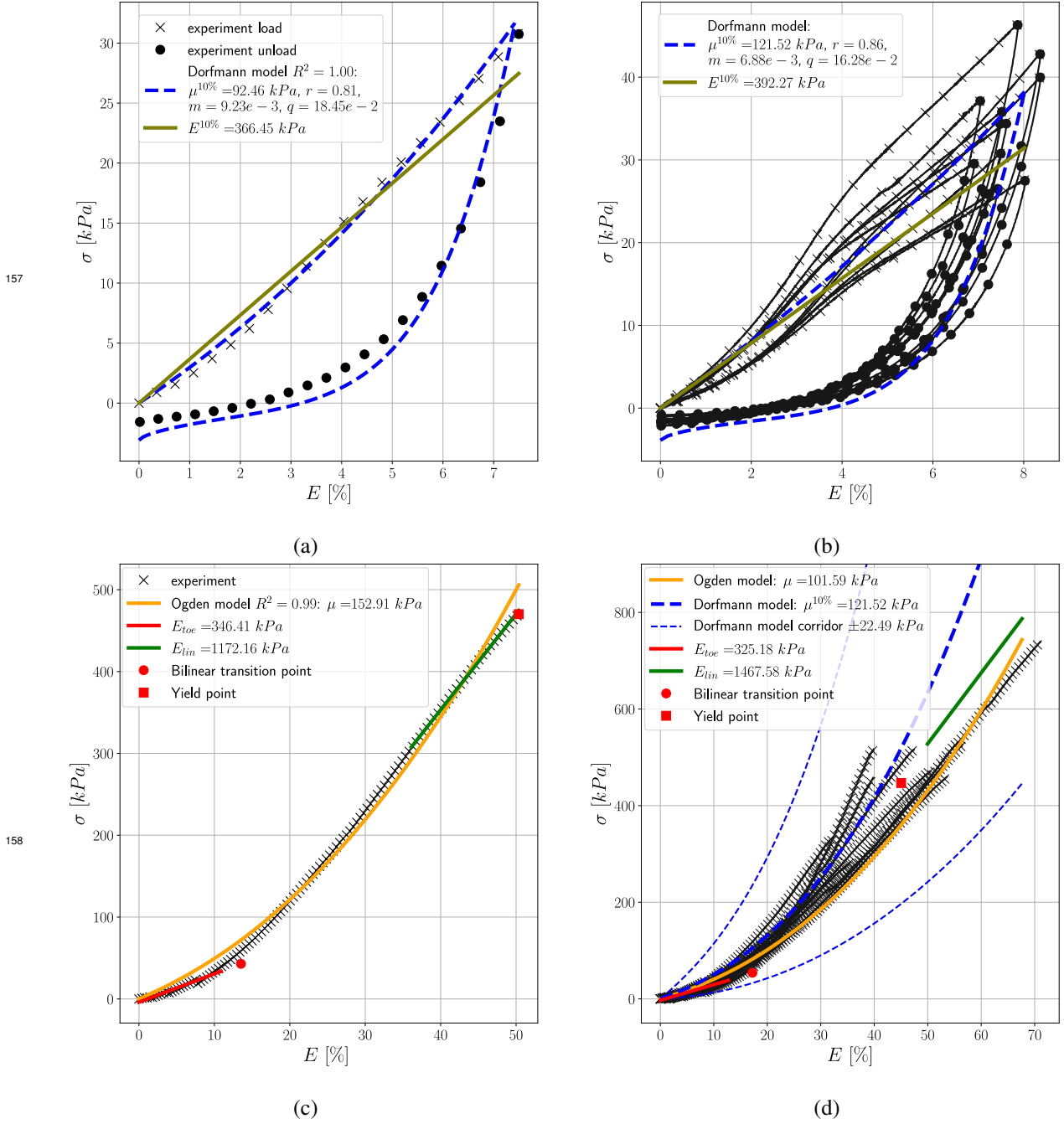
(a)

(b)

(c)

(d)

Figure 4: Characterization over step 4 and 5. a) gives the results for the same representative sample (160206_E4) with the linear elastic behavior represented thanks to the olive green continuous line while the dashed blue line is related to the Dorfmann model fitting. Extended to the whole database on b) allows appreciating the average fitting quality. Step 5 corresponds to a load up to sample yield given by the red square point. c) is dedicated to the representative sample (160206_E4) highlighting the bilinear characterization with toe and linear region respectively red and green lines with the red dot transition point. The nonlinear response has been fitted with the Ogden model represented by the orange line. Finally, d) is the averaging extension over the whole database on which average results of step 4 characterization have been added in dashed blue line with the uncertainty corridor.

160   Note that next to the grip system, the specimen is subjected to a concentration and a triaxiality of stresses. This

161   phenomenon is especially present for large deformations and is beyond the scope of this study. Once the stress σ and

162   strain E curve have been calculated, associated to this stage, yield stress σ_y and strain E_y have been registered and

163   appear in table 1. This latter table gathered all material parameters, i.e. based on the experimental data and not related

164   to a model, while the table 2 is dedicated to the models' ones. The linear and bilinear characterizations have been

165   performed on both steps of interest, respectively 4 and 5, leading to plots presented in figure 4 and parameters values

166   recorded in table 2. For better appreciation of characterization procedure, a representative sample (160206_E4) has

167   been presented on figures 3, 4.a and 4.c, while the average results have been plotted overall database on figures 4.b

168   and 4.d. The monotone strain loading from 0 to 8 % induced an almost linear behavior ($E_{toe}^{10\%} = E_{lin}^{10\%} = E^{10\%}$) which

169   is appreciated on figure 4.a and 4.b by the olive green straight line. This statement is confirmed by the step 5 curves

170   (cf. bilinear transition point in figure 4.d) where the average transition point, in between "toe" and "linear" regions,

171   is obtained at $E_T = 17.22$ % strain related to $\sigma_T = 56.67$ kPa. Figures 4.c and 4.d plots show a clear transition in

172   between the regions with a 5.7 factor from E_{toe} to E_{lin} confirming the expected non linear behavior of the WJ samples.

173

Δl [%]	ρ [$kg.m^{-3}$]	σ_y [kPa]	E_y [%]	E_T [%]	σ_T [kPa]
13.13 ± 4.79	36.13 ± 4.95	446.76 ± 147.75	45.03 ± 13.54	17.22 ± 4.33	56.67 ± 25.47

174   Table 1: Material parameter data (*mean ± S D, n = 10*)

175   Using the three terms model of Ogden (1972) as well as the extension developed by Dorfmann and Ogden (2004),

176   both last loading steps (4 and 5) have been reproduced as shown on figure 4 subplots. The optimization over the whole

177   database led to obtain the average parameters values gathered in table 2.

178

μ_1 [kPa]	α_1 [$-$]	μ_2 [kPa]	α_2 [$-$]	μ_3 [kPa]	α_3 [$-$]	μ [kPa]
-604.01 ± 118.54	0.65 ± 0.16	49.49 ± 6.86	5.79 ± 3.11	47.94 ± 8.77	6.72 ± 2.15	101.59 ± 43.13
$\mu_1^{10\%}$ [kPa]	$\alpha_1^{10\%}$ [$-$]	$\mu_2^{10\%}$ [kPa]	$\alpha_2^{10\%}$ [$-$]	$\mu_3^{10\%}$ [kPa]	$\alpha_3^{10\%}$ [$-$]	$\mu^{10\%}$ [kPa]
-615.05 ± 170.63	0.62 ± 0.18	51.66 ± 10.25	7.81 ± 0.93	35.45 ± 15.10	6.69 ± 2.33	121.52 ± 22.49
r [$-$]	m [$\times 10^{-3}$ $-$]	q [$\times 10^{-2}$ $-$]	$E^{10\%}$ [kPa]	E_{toe} [kPa]	E_{lin} [kPa]	
0.86 ± 0.06	6.88 ± 1.33	16.28 ± 2.64	392.27 ± 65.91	325.18 ± 75.51	1467.58 ± 440.05	

180   Table 2: Model parameter data (*mean ± S D, n = 10*)

181   All data was used to plot correlation matrices and perform principal component analysis (PCA). The global matrix

182   is provided in Appendix B and the figure 5 presents a reduced matrix with strong absolute correlations (i.e. higher
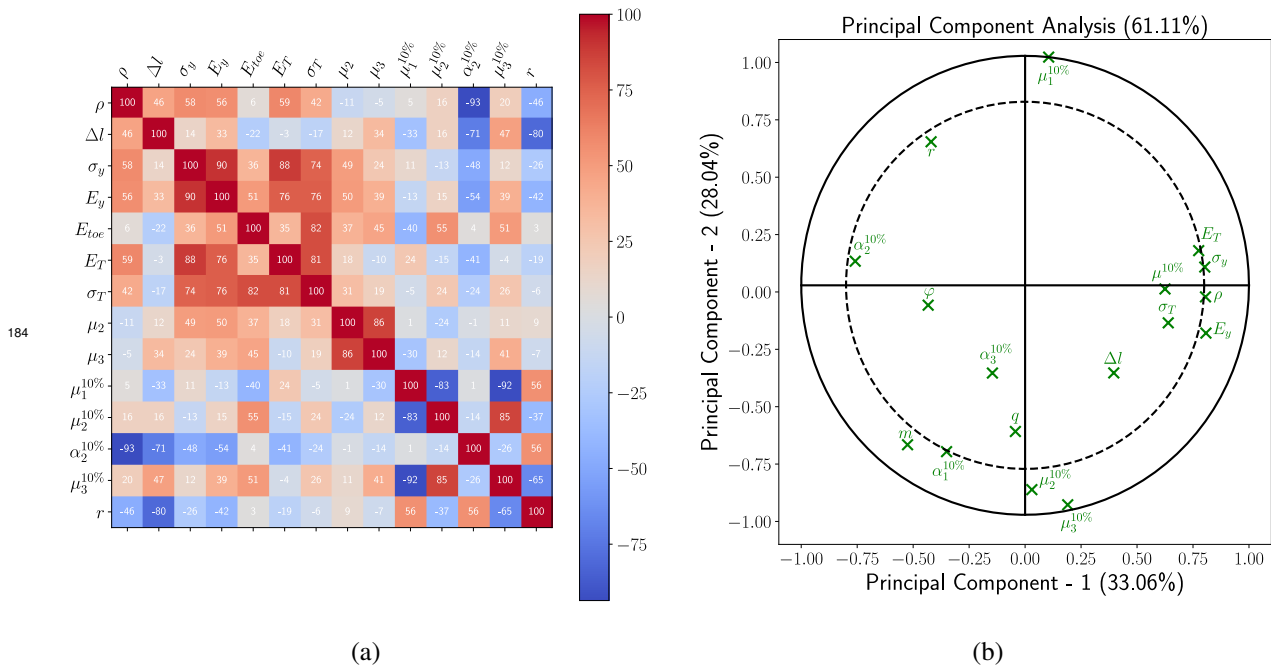
183   than 80 %).

Figure 5: a) Correlation matrix with strong correlations ($\geq 80\%$) and b) PCA normalized correlation circle on material and Dorfmann and Ogden (2004) parameters the dash line represents the 80% threshold

Material parameters such as density ρ, yield $\left(\sigma_y, E_y\right)$ and transition $\left(\sigma_T, E_T\right)$ points as well as relative length variation Δl present high correlations meaning consistent criteria of the WJ mechanical behavior. Actually, it is noteworthy that transition and yield points are strongly linked (≥ 74 %). The linear characterizations are revealing their limits with only one parameter E_{toe} strongly linked (86%) to the transition stress σ_T. Moreover, the linear model parameters appear to be correlated ($\geq 70\%$ in Appendix B) to the non-linear ones giving confidence to the obvious progression from linear to non-linear modeling. The model of Ogden (1972) gathers two self correlated parameters (μ_1 and μ_2) and weak correlation with the material parameters ($\leq 66\%$ in Appendix B) while Dorfmann and Ogden (2004) model shows high correlations. For this latter model, self correlations are numerous but fitting parameters $\alpha_2^{10\%}$ and r are respectively linked to material parameters ρ (93% absolute) and Δl (80% absolute). For accurate analysis, a correlation circle on material and Dorfmann and Ogden (2004) parameters has been plotted in figure 5.b. Being 61.11% representative, while 60.41% for Ogden (1972) one given in Appendix B, it confirms the previous results. Most of the Dorfmann and Ogden (2004) parameter being farther from the circle center attests the identification quality over database. In addition, it exhibits an interesting 2D balanced plane where material parameters, including the identified shear modulus $\mu^{10\%}$, contribute to the first axis (33.06%) and model parameters to the second axis (28.04%) with the anti-correlation between the fitting parameter r and the relative length variation Δl linking them.

4. Discussion

Wharton's Jelly tissue constitutes a promising scaffold in tissue healing and regenerative medicine. However, its use in an allogenic situation implies a reduced immunogenicity, which could be hampered by a high content in nucleic content (i.e. > 50 ng/mg of tissue). Herein, the extracted nucleic moieties were below 50 $ng/mg/\mu L$, threshold fixed by European Medicines Agency. For a better tissue preservation and medical application, WJ was freeze-dried (Mellor, 1975; Nakamura et al., 2008; Tsujimoto et al., 2020). Herein, the mechanical behavior of rehydrated WJ in PBS was determined. The porosity, φ, assessment is in agreement with the literature (Gervaso et al., 2014; Sloper et al., 1979) as well as the related progressive transparency shown in figure 2.b (Safari et al., 2019).

In spite of the WJ harvest, the resulting viscous nonlinear elastic behavior obtained is fully in tune with the literature (Gervaso et al., 2014; Pennati, 2001). Even though microscopic material heterogeneities observed and mentioned in the literature, the current results obtained, for random donors, locations and orientations, are presenting a good reproducibility overall database. The maximum relative uncertainty ($S D / |mean|$)) on material parameters is below 45 % and related to the bilinear stress transition σ_T. Besides relieving this macroscopic analysis from microstructural noticeable influences, it points out database quality.

Withstanding strain loading up to $E_y = 45.03$ % on average, WJ exhibited $\sigma_y = 446.76$ kPa yield stress. These values are respectively higher and lower than the ones presented by Pennati (2001) (even considering engineering strain as Pennati (2001) the loading strain is higher with a value of 37.55%). This divergence is related to various factors such as donor variability and sample processing as well as test conditions. In Pennati (2001) work, tensile tests were performed at 23.5 ± 2^oC within a $61 \pm 12\%$ humid environment. In our case, being closer to physiological conditions, it is consistent to obtain a more compliant mechanical response due to full hydration and 37^oC temperature. Like other studies (Franceschini et al., 2006; Pennati, 2001), failure characterization remains difficult to control through uniaxial tensile load experiment due to sample small dimensions and high strain load. Appearing in between glued dry material and hydrated one (cf. figure 2.c), the evaluated yield point $\left(E_y, \sigma_y\right)$ is certainly underestimated compared to a fully hydrated sample without dry/wet interfaces. Although, it remains an important result for clinical applications where interfaces might appear while fixing biomedical devices with membrane shape. For an accurate characterisation of the yield point, finite element simulation could be used to reproduce the experiment and more precisely the boundary conditions at the fixation point.

Linear and bilinear characterization results are in between Pennati (2001) and Gervaso et al. (2014) ones. An explanation for our higher values compared to Gervaso et al. (2014) is the fact that, for tensile test, we can not control how much material fibers are recruited while in confined compression they do not play any role. Being in the range of literature results, these characterization results are confirming the experiment quality. The mechanical step-through brought by this work comes from the analytical nonlinear characterization over a cyclic load which, from author knowledge, is new and promising for WJ finite element simulations (Brunelli et al., 2019). Applying classical Ogden (1972) model to fit the step 5 behavior yields obtaining a shear modulus of $\mu = 101.59$ kPa. Considering an

incompressible material due to WJ high water content would give a Young's modulus three times higher which is also consistent with above discussion. Due to WJ repeatable response, automated parameter identification gave trustful results with a maximum relative uncertainty of 53.80 % on the α_2 fitting parameter. Taking into account the viscous behavior with Dorfmann and Ogden (2004) model allowed reducing this value to 42.61 % affecting the $\mu_3^{10\%}$ fitting parameter. Comparing models' shear moduli μ and $\mu^{10\%}$, points out a higher value for Dorfmann and Ogden (2004) model, $\mu^{10\%}$= 121.52 kPa, which is consistent with the superimposed material viscosity damping the hyperelastic response. To confirm the quality of this latter accurate model, the identified behavior and its corridor have been extended and plotted with dashed blue lines on figure 4.d. Besides, these parameters values are well below the ones obtained by Karimi and Navidbakhsh (2014) for umbilical cord's arteries and vein that have an order of magnitude in MPa. It is consistent with the literature as WJ aims to embed these vessels while damping mechanical loads applied on the whole umbilical cord.

Even though Dorfmann and Ogden (2004) model exhibits self-correlated parameters, leading discussing model quality in term of parameter physical meaning, its parameters present higher correlations to the material parameters than the Ogden (1972) ones. Once again focusing on shear moduli within the full Pearson's correlation matrix (cf. Appendix B.a), $\mu^{10\%}$ presents higher correlation values with material parameters than μ. The correlation circle confirmed the confidence given to Dorfmann and Ogden (2004) identification. Its parameters being farther from the circle center highlights a good representativeness leading to a global shear modulus closer to the first axis dedicated to material parameters. Nonetheless, the low individual correlation or anti correlation of nonlinear models' parameters points out their limitations to connect with material properties hidden by their strong ability to fit non-linearity.

From PCA, an interesting observation to predict sample yield behavior is the "toe" region slope E_{toe}. In fact, being 82 % linked to the transition stress σ_T, whose correlation to yield stress σ_y and strain E_y are respectively 74 % and 76 %, gives a predictive indication on sample failure. In fact, it represents an indication to predict WJ mechanical response. The anti-correlation in between the fitting parameter r and the relative length variation Δl (−80 %) highlights the coupling in between hydration and viscous behavior. It completes the literature where this poro-mechanical interaction has been studied for confined compression tests (Gervaso et al., 2014) and observed for tensile relaxation test (Pennati, 2001). Nonetheless, the material viscosity is certainly also related to the collagen solid phase viscosity which is under current investigation.

Regarding the experimental procedure, these results will help designing improved protocols for instance taking into account the hydration effect on sample geometry. In fact, a weakness of the presented procedure is the evaluation of the sample thickness after hydration that has been considered equal to the dry one being the lowest sample dimension. The use of image analysis such as digital image correlation would definitely allow collecting more data especially for large strain loads. Although, the optical flow is really difficult to maintain due to various media on the optical path and hydration effect as mentioned earlier. The use of markers to tackle this issue is also controversial due to the sample thinness as well as its low stiffness. Actually, adding markers could affect the mechanical response of such WJ membranes. Out of the scope of this paper but interesting for future investigation, these results open the possibility

270 to assess the effect of the freeze drying procedure even though performing uniaxial tensile tests on fresh WJ might be

271 complex to set up.

5. Conclusions

273 WJ viscous nonlinear mechanical response has been investigated while undergoing cyclic and ultimate tensile

274 loads. In addition to the well-known biological features, herein, the WJ mechanical repetitiveness confirms the interest

275 of such a material for regenerative medicine. A side of the knowledge improvement on WJ mechanical response, this

276 paper provides accurate data that will enhance predictive simulation work such as finite element analysis. In fact,

277 both Ogden's model and its improved version efficiently reproduce the experimental results opening ways to also use

278 more complex models. Principal component analysis confirmed their high quality fitting ability. However it also

279 highlights that models' physical parameters constitute a limit for multiscale understanding of WJ behavior. Indeed,

280 WJ is a highly hydrated connective tissue. Although, the current protocol was conducted in environment close to

281 physiological situation, further investigations on hydro-chemo-mechanical couplings should be considered to deeply

282 decipher the GAG and hydration role in the mechanical behavior of WJ.

Author contributions

286 **Adrien Baldit:** Conceptualization; Data curation; Formal analysis; Investigation; Methodology; Project administra-

287 tion; Resources; Supervision; Validation; Visualization; Writing - original draft and review & editing.

288 **Marie Dubus:** Conceptualization; Data curation; Formal analysis; Investigation; Methodology; Resources; Valida-

289 tion; Visualization; Writing - original draft.

290 **Johan Sergheraert:** Conceptualization; Investigation; Resources; Validation; Writing - original draft.

291 **Halima Kerdjoudj:** Conceptualization; Formal analysis; Funding acquisition; Project administration; Supervision;

292 Validation; Writing - review & editing.

293 **Cedric Mauprivez:** Conceptualization; Supervision; Validation; Writing - review & editing.

294 **Rachid Rahouadj:** Conceptualization; Formal analysis; Funding acquisition; Methodology; Supervision; Valida-

295 tion; Writing - review & editing.

Appendix A. Visco hyperelastic python script

The script `Baldit_YEAR_JMBBM_Dorfmann_2004_script.py` allows plotting both Dorfmann and Ogden (2004) and current work curves with the same function confirming the method quality.
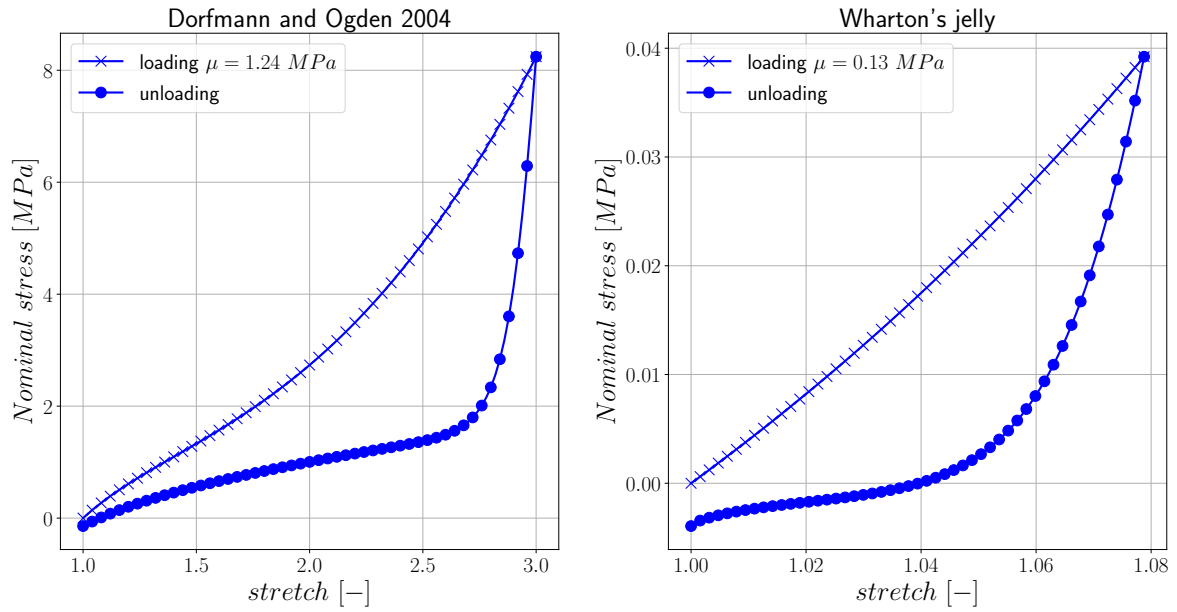
It is available on `gitlab.univ-lorraine.fr` (once the work is accepted) for readers to try this procedure for their experimental or modelling data.

Appendix B. Statistical analysis

(a)
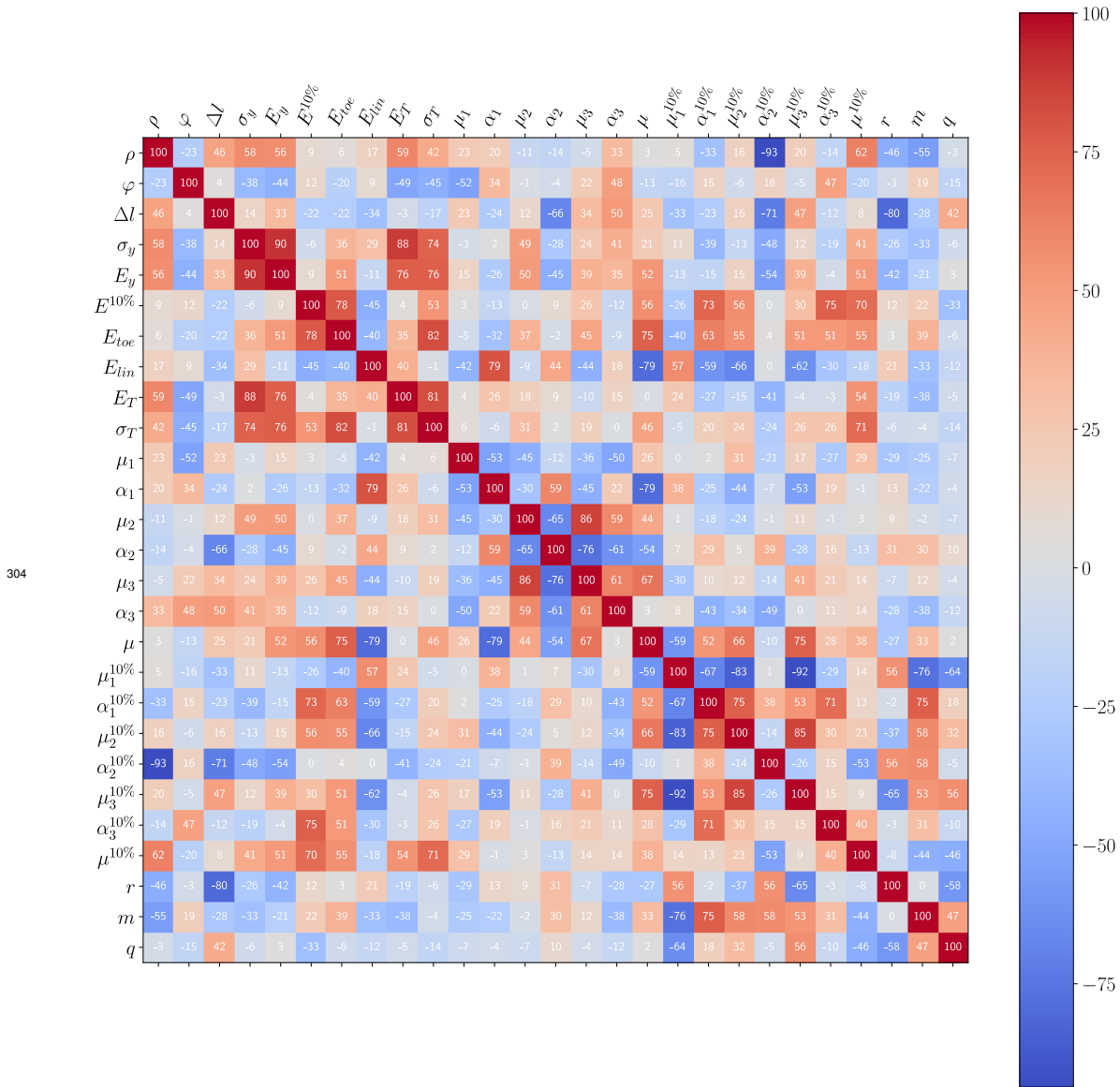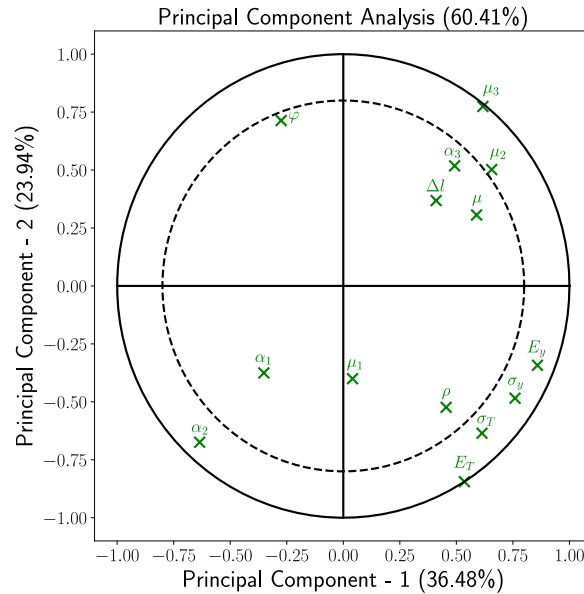
(b)

Figure B.6: a) Full Pearson's correlation matrix and b) PCA normalized correlation circle on material and Ogden (1972) parameters the dash line represents the 80% threshold

References

Baldit, A., Ambard, D., Cherblanc, F., Royer, P., 2014. Experimental analysis of the transverse mechanical behaviour of annulus fibrosus tissue. Biomechanics and Modeling in Mechanobiology 13, 643–652.

Brunelli, R., De Spirito, M., Giancotti, A., Palmieri, V., Parasassi, T., Di Mascio, D., Flammini, G., D'Ambrosio, V., Monti, M., Boccaccio, A., Pappalettere, C., Ficarella, E., Papi, M., Lamberti, L., 2019. The biomechanics of the umbilical cord wharton jelly: Roles in hemodynamic proficiency and resistance to compression. Journal of the Mechanical Behavior of Biomedical Materials 100, 103377.

Caputo, W.J., Vaquero, C., Monterosa, A., Monterosa, P., Johnson, E., Beggs, D., Fahoury, G.J., 2016. A retrospective study of cryopreserved umbilical cord as an adjunctive therapy to promote the healing of chronic, complex foot ulcers with underlying osteomyelitis. Wound Repair and Regeneration 24, 885–893.

Dorfmann, A., Ogden, R.W., 2004. A constitutive model for the mullins effect with permanent set in particle-reinforced rubber. International Journal of Solids and Structures 41, 1855 – 1878.

Fernandez, D., 2019. Cryopreserved amniotic membrane and umbilical cord for a radiation-induced wound with exposed dura: a case report. Journal of Wound Care 28, S4–S8.

Franceschini, G., Bigoni, D., Regitnig, P., Holzapfel, G., 2006. Brain tissue deforms similarly to filled elastomers and follows consolidation theory. Journal of the Mechanics and Physics of Solids 54, 2592 – 2620.

Gervaso, F., Boschetti, F., Pennati, G., 2014. Evaluation of the wharton's jelly poroelastic parameters through compressive tests on placental and foetal ends of human umbilical cords. Journal of the Mechanical Behavior of Biomedical Materials 35, 51 – 58.

Gluckman, E., Broxmeyer, H.A., Auerbach, A.D., Friedman, H.S., Douglas, G.W., Devergie, A., Esperou, H., Thierry, D., Socie, G., Lehn, P., 1989. Hematopoietic reconstitution in a patient with fanconi's anemia by means of umbilical-cord blood from an hla-identical sibling. 321, 1174–8.

327 Gupta, R., Turati, V., Brian, D., Thrussel, C., Wilbourn, B., May, G., Enver, T., 2020. Nov/ccn3 enhances cord blood engraftment by rapidly
328   recruiting latent human stem cell activity. Cell Stem Cell .

329 Herndon, D.N., Branski, L.K., 2017. Contemporary methods allowing for safe and convenient use of amniotic membrane as a biologic wound
330   dressing for burns. Annals of Plastic Surgery 78.

331 John, S., Kesting, M.R., Paulitschke, P., Stöckelhuber, M., von Bomhard, A., 2019. Development of a tissue-engineered skin substitute on a base
332   of human amniotic membrane. Journal of Tissue Engineering 10, 1–14.

333 Karimi, A., Navidbakhsh, M., 2014. A comparative study on the uniaxial mechanical properties of the umbilical vein and umbilical artery using
334   different stress–strain definitions. Australasian Physical & Engineering Sciences in Medicine 37, 645–654.

335 Knudtzon, S., 1974. In Vitro Growth of Granulocytic Colonies From Circulating Cells in Human Cord Blood. Blood 43, 357–361.

336 Kočí, Z., Výborný, K., Dubišová, J., Vacková, I., Jäger, A., Lunov, O., Jiráková, K., Kubinová, u., 2017. Extracellular matrix hydrogel derived from
337   human umbilical cord as a scaffold for neural tissue repair and its comparison with extracellular matrix from porcine tissues. Tissue Engineering
338   Part C: Methods 23, 333–345.

339 Mallis, P., Boulari, D., Chachlaki, P., Giokas, C.S., Michalopoulos, E., 2020. Vitrified wharton's jelly tissue as a biomaterial for multiple tissue
340   engineering applications. Gynecological Endocrinology 36, 139–142.

341 Marston, W.A., Lantis 2nd, J.C., Wu, S.C., Nouvong, A., Lee, T.D., McCoy, N.D., Slade, H.B., Tseng, S.C., 2019. An open-label trial of cryop-
342   reserved human umbilical cord in the treatment of complex diabetic foot ulcers complicated by osteomyelitis. Wound Repair and Regeneration
343   27, 680–686.

344 Mechiche Alami, S., Velard, F., Draux, F., Siu Paredes, F., Josse, J., Lemaire, F., Gangloff, S., Graesslin, O., Laurent-Maquin, D., Kerdjoudj, H.,
345   2014. Gene screening of wharton's jelly derived stem cells. Biomed Mater Eng , 53–61.

346 Mellor, J.D., 1975. Fundamentals of Freeze Drying. London : Academic Press.

347 Nakamura, T., Sekiyama, E., Takaoka, M., Bentley, A.J., Yokoi, N., Fullwood, N.J., Kinoshita, S., 2008. The use of trehalose-treated freeze-dried
348   amniotic membrane for ocular surface reconstruction. Biomaterials 29, 3729 – 3737.

349 Ogden, R.W., 1972. Large deformation isotropic elasticity - on the correlation of theory and experiment for incompressible rubberlike solids.
350   Proceedings of the Royal Society of London. A. Mathematical and Physical Sciences 326, 565–584.

351 Pennati, G., 2001. Biomechanical properties of the human umbilical cord. Biorheology .

352 Raphael, A., 2016. A single-centre, retrospective study of cryopreserved umbilical cord/amniotic membrane tissue for the treatment of diabetic
353   foot ulcers. Journal of Wound Care 25, S10–S17.

354 Safari, F., Fani, N., Eglin, D., Alini, M., Stoddart, M.J., Baghaban Eslaminejad, M., 2019. Human umbilical cord-derived scaffolds for cartilage
355   tissue engineering. Journal of Biomedical Materials Research Part A 107, 1793–1802.

356 Sloper, K., Brown, R., Baum, J., 1979. The water content of the human umbilical cord. Early Human Development 3, 205 – 210.

357 Tappert, L., Baldit, A., Nascimento, R.D., Lipinski, P., Rahouadj, R., 2018. Mechanical characterisation of the temporomandibular joint disc
358   through local compression and traction, in: BSSM 2018 Congress.

359 Tettelbach, W., Cazzell, S., Sigal, F., Caporusso, J.M., Agnew, P.S., Hanft, J., Dove, C., 2019. A multicentre prospective randomised controlled
360   comparative parallel study of dehydrated human umbilical cord (epicord) allograft for the treatment of diabetic foot ulcers. International Wound
361   Journal 16, 122–130.

362 Tsujimoto, Y., Kaneko, T., Yoshida, T., Kimura, K., Inaba, T., Sugiura, K., Hatoya, S., 2020. Development of feline embryos produced using
363   freeze-dried sperm. Theriogenology 147, 71 – 76.